Calcium Transients in Dendritic Spines

Ekta Dadlani, Shayan Raofi, and Tyler Bodily

Abstract

In this report, we modify a deterministic model showcasing calcium transients in dendritic spines through various sources and sinks as a system of partial differential equations. We consider boundary conditions at the plasma membrane, the neck, and the spine apparatus (an extension of the endoplasmic reticulum) to model the diffusion of cytosolic calcium in specified spine geometries. All models were designed through COMSOL.The original model, published by Bell et. al., considered a short time scale (10-100ms), considered the spine apparatus of the spine primarily as a sink for cytosolic calcium, and treated the calcium at the base of the dendritic spine neck as an isolated, or clamped system. We strived towards developing a more physiological approach to model the cascade of calcium through the dendritic spine by implementing a longer time scale (10ms-15s), adding ryanodine receptors to incorporate a source of calcium in the spine apparatus, adding an efflux term at the base of the dendritic spine neck, and modeling additional geometries. Increasing the time scale allowed us to visualize the long lasting effects of the neck efflux and the ryanodine receptors. The neck efflux allowed us to treat the base of the neck as a dynamic system, confirming the localization of calcium within the spine. The incorporation of the ryanodine receptors allowed us to analyze the dominating effects of the spine apparatus and determine that its role in calcium dynamics shifts between being a sink in short and long timescales and a source in intermediate timescales. We considered modeling long-thin spines and stubby spines as a way to examine how other biologically relevant spine geometries behave. In doing so we also re-emphasized the importance of the surface area to volume ratio of the spine in determining calcium dynamics as found in the original paper by Bell et al..

Background

Neurons are known to communicate with each other via synapses by sending chemical signals to each other from the axon of the sending neuron, the presynaptic neuron, to the dendrite of the receiving neuron, the postsynaptic neuron. An action potential, or an electrical stimulus, triggers release of neurotransmitter from the presynaptic neuron at the synaptic cleft. The neurotransmitters stimulate the postsynaptic neuron by binding to ligand-gated receptors, inducing an electrical stimulus via ionic currents driven by membrane potential. While much is known about the larger picture of this extensive process, researchers have been investigating the more intricate structures that are affected during the process of learning and memory that result from neuronal signals.

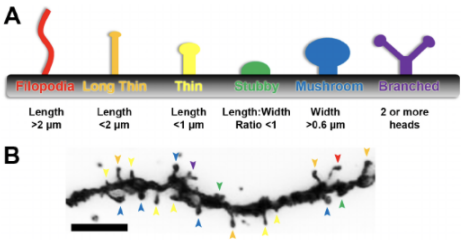

Figure 1. Overview of Dendritic Spine Geometry

At the heart of this research concerning learning and memory are dendritic spines. Dendritic spines are small protein and actin rich protrusions along the length of the dendrites of neurons. They generally consist of a neck region and head region, though other morphologies exist[14]. It plays a critical role in calcium influx and membrane depolarization, resulting in action potential generation along the length of the dendrite. We have chosen to focus on a recent model describing calcium transport within the dendritic spine while considering places of calcium flux along the plasma membrane and spine apparatus (SpApp) by Bell et al..

The spine head can have a variety of different shapes, from a sphere, to ellipse/mushroom, to filopodia. Dendritic spines generally form excitatory synapses and function as the postsynaptic means for synaptic transmission. On average, there exists ~40,000 spines on 280 apical dendritic branches[17]. Each spine contains structural components that allow each one to act as its own isolated signaling subcompartment of the dendrite. The number of spines and their shapes vary from branch to branch and are often proportional to the strength of a synapse, which is why these protrusions are important for learning and memory. Calcium is a key player in modifying dendritic spines during synaptic plasticity, as it triggers both immediate responses and long term responses that strengthen the synapse. The paper we are building upon concluded that “the volume-to-surface area ratio of the spine regulates calcium dynamics”[2]. Larger spines tended to imply stronger synapses[2].

Given that calcium is so important to synaptic plasticity, it is important to study how its concentration evolves during synaptic transmission. However, since spines are so small, around 0.06um^3, it is difficult to use fluorescent tags to monitor calcium levels. This is because the calcium concentration is low enough that the tags start acting as significant calcium buffers–reducing the actual amount of calcium in the spine and changing the spine's response. Therefore, computational models are used to study these dynamics[2].

Methods

Biological Relevance

Time

The original model focused on very short time scales (10-100 ms) and didn't account for longer time scale dynamics such as SpApp calcium release via IP_3 receptors, ryanodine receptors (RYR), and calcium-induced-calcium release channels (CICR)[2]. RyR begins working within the 10-100ms time range, and can have longer lasting effects. Furthermore, we wanted to visualize the flow of calcium out of the spine head through the neck. As such, in order to make sure we captured these phenomena, we increased the time scale from 100 ms to 15 seconds[7].

Membrane Voltage

The basis of calcium released in the spine was modeled by a depolarization of the membrane voltage. This depolarization is the summation of an excitatory postsynaptic potential (EPSP), which would normally be caused by neurotransmitter released by the presynaptic neuron, and back-propagating action potential (BPAP), which is an action potential within the postsynaptic neuron that travels backwards from the soma to the dendrites[2]. In this way there is a maximal depolarization of the dendritic spine. BPAPs have been shown to reach the spines at an average of 2ms after an EPSP[2].

Head Geometry

There is a wide range of dendritic spine shapes that can correlate to different biological conditions and situations. Two of the most common were focused on within the original model, the spheroid and ellipsoid (mushroom) models. Spheroid models seem to be more prevalent in new synapses whereas mushroom head geometries are more common in mature synapses. In general, as the spine progresses in maturity, it changes from a filopodia structure to wide-headed mushroom shaped spines[14]. Our improved model not only focused on the original spheroid and ellipsoid models, but also included modified head geometries that better cover the range of potential head shapes. We included models of long thin neck spines with and without spine apparatus and stubby spines with short necks, as showcased in the supplementary material in sections S6, S7, and S10.

Spine Apparatus Geometry

Some dendritic spines have an organelle called the Spine Apparatus (SpApp). This organelle is similar to the sarcoplasmic reticulum. The spine apparatus can absorb and store calcium from the cytoplasm as well as release it, so it has properties of both a calcium sink and calcium source. The main way it acts as a source is through Ca^{2+}-induced-Ca^{2+}-release, (CICR), and can spread signals throughout the cell[3,10,17]. It also plays a role in regulating spine volume. Larger spine heads and geometries tend to have a SpApp, but it is not as common in smaller or thinner dendritic spines. We tested the small, stubby geometry without an SpApp and tested the larger, long thin morphology with and without it the SpApp. The original model tested the ellipsoid and spherical head geometry with and without a spherical SpApp; we tested these morphologies as well[2]. Assuming a spheroid geometry for the spine apparatus is an oversimplification, but studies have shown that the dimensions of the spine apparatus are often comparable with the dimensions of the spine head[16].

Mathematical Approach

Boundary Flux at the Spine Apparatus

The fluxes at the SpApp included in the original paper were the fluxes through SERCA pumps and leak channels. SERCA pumps are used to transport calcium from the intracellular space of the dendrite into the spine apparatus; it is dependent on cytosolic calcium concentration and kinetic parameters. A small leak flux term is added to account for the leak current from the spine apparatus to the cytoplasm; this term offsets the

SERCA pump at the basal calcium concentration (100 nM). The leak term is based on the difference in cytosolic calcium concentration and the concentration of calcium in the ER. These channels were uniformly spread along the SpApp volume. Thus, the boundary condition for the SpApp in the original model was:

$$-D(n * \nabla Ca)|_{SpApp} = J_{SERCA} - J_{LEAK}$$

Equation 1: Boundary conditions and fixed fluxes at the Spine Apparatus Membrane as presented in Bell et. al.

$$J_{SERCA} = \frac{\beta_i \beta_{SERCA} n_{SpApp_r} V_{maxr19} [Ca^{2+}]^2_{cyto}}{K^2_{Pr19} + [Ca^{2+}]^2_{cyto}}$$

Equation 2: SERCA flux. The flux of Ca^{2+} from the extracellular space to the Spine Apparatus via the SERCA pumps is dependent on the cytosolic calcium concentration, Ca^{2+} buffering, voltage change, and the ratio of the SpApp volume to the SpApp membrane surface area.

$$J_{leak} = k_{leak} n_{SpApp_r} \left([Ca^{2+}]^2_{ER} - [Ca^{2+}]^2_{cyto} \right)$$

Equation 3: Leak Flux. The leak of Ca^{2+} from the Spine Apparatus to the cytosol is used to balance the pump terms of basal Ca^{2+} concentrations.

The Spine Apparatus is known as a source for calcium through the release of Ca^{2+} ions at longer timescales (10 ms-100 ms). This release is based on CICR through ryanodine receptors (RyR)[2,16]. CICR is a process in which calcium release from intracellular calcium stores is promoted by the presence of increased cytosolic calcium; it provides amplification of the propagation of calcium signals and increases the speed of the diffusion of calcium[15]. RyR are receptors located in the neck and the head, which release calcium internally from the spine apparatus into the spine[1]. CICR is usually initiated post depolarization, which lets in an initial concentration of calcium into the cytosol through voltage gated channels[3,6]. These receptors bind selectively with ryanodine and release calcium as sparks.

We incorporated RyRs by adding an additional term to showcase the Ca^{2+} flux from the endoplasmic reticulum to the cytosol along the entire SpApp[12,16]. The set of equations models the kinetics of RyR by considering the non diminishing equilibrium open probability of the receptors on a slowed timescale. The kinetics of RyRs were developed using Hill-type approximations, which is often used to model multimeric proteins[10,12]. This calcium flux, as introduced in Leung et. al and Keizer et. al., is added to the original paper's SpApp boundary condition and is spread uniformly across the SpApp volume:

$$J_{RYR} = (V_{RYR} P_O + V_{LEAK})(Ca^{2+}_{ER} - Ca^{2+}_{cyto})$$

Equation 4: The flux of Calcium from the spine apparatus to the cytosol via ryanodine receptors, where V_{RYR} is the rate of Ca^{2+} flux from the ER to the cytosol via the RyR, P_o is the open probability of RyR (dependent on the Ca_{cyto} concentration because this is a CICR dependent process), and V_{leak} is the rate of the leak of Ca^{2+} from the ER. Equation from Leung et. al.

$$-D(n * \nabla Ca)|_{SpApp} = J_{SERCA} - J_{LEAK} - J_{RYR}$$

Equation 5: Addition of the Ca2+ flux via the Ryanodine receptors (as a sink) to the Spine Apparatus Membrane at the neck and the head of the model.

The SpApp starts with 60uM of calcium.

Cytosolic Flux

Calcium entering the spine will both diffuse through the cytosol and bind to various molecules, which act as calcium buffers. As such the cytosolic flux was modeled as a reaction diffusion equation:

$$\frac{\partial [Ca^{2+}]}{\partial t} = D_{Ca^{2+}} \nabla^2 [Ca^{2+}] - f(Ca^{2+}, CBP)$$

Equation 6. Cytosolic Reaction Diffusion. Ca^{+2} is the cytosolic calcium content.

The buffers are thought to be free cytosolic buffers and fixed buffers. The identities of these buffers are not well cataloged. It is speculated that the fixed buffers could be receptors for channel modulation and secondary messenger pathways. The mobile buffers are completely unknown; however, their dynamics have been studied and they can therefore be modeled as diffusive molecules[2,4]. Thus, the reaction component of the equation was broken up into two parts, a fixed buffer component which will be added to the plasma membrane flux (in the next section), and a diffusive buffer component that was added to the reaction diffusion equation:

$$\frac{\partial[Ca^{2+}]}{\partial t} = D_{Ca^{2+}}\nabla^2[Ca^{2+}] - k_{B_{m,on}}[Ca^{2+}][B_m] + k_{B_{m,off}}[CaB_m]$$

Equation 7. Reaction diffusion equation with fixed buffers and diffusive component. B_m is the mobile buffer and CaB_m is the mobile buffer bound to calcium. Calcium binding and unbinding to the buffer is based off reaction equations and markov kinetics: $[Ca^{2+}] + [B_m] \rightleftharpoons [CaB_m]$ in which the forward rate constant is $k_{Bm,on}$ and the reverse rate constant is $k_{Bm,off}$.

The cytosolic calcium concentration is almost fully dependent on the boundary condition fluxes, as the initial condition for calcium concentration is 100nM, consistent with studies regarding the intracellular concentration of ions. These equations are unchanged from the original Bell et al. paper.

Plasma Membrane Boundary Condition

The plasma membrane acts as the barrier between the extracellular space and the intracellular cytosol. The extracellular space has a much greater number of calcium ions than the intracellular space at any given time. Therefore, the extracellular space can be modeled as an infinite source of calcium ions. Calcium intake is triggered by an excitatory postsynaptic potential (EPSP) at time t=0s and backpropagating action potential (BPAP) at time t=2ms [2].

Flux into the spine is mediated by N-methyl-D-aspartate receptors (NMDARs) and voltage sensitive calcium channels (VSCC). NMDARs are nonspecific cation channels. They are coincidence detectors, thus, they open upon binding to glutamate if the membrane voltage has crossed a threshold; glutamate binding often coincides with membrane depolarization since it is the primary excitatory neurotransmitter, and as such was abstracted to be part of the EPSP. NMDAR response is graded, it confers more current at voltages higher than its threshold, so the calcium flux is reinforced by the BPAP. This ensures maximum calcium current[2]. NMDARs are found in an area on the apex of the spine, the postsynaptic density (PSD). The PSD was set to be a fixed proportion of the spine head surface area. NMDARs were uniformly distributed across the PSD at a high concentration. VSCCs respond to the depolarization by both the EPSP and BPAP and are uniformly distributed across the entire plasma membrane. Their calcium current and opening times were based on previous modeling studies in which their gating parameters were fit to a biexponential[2].

$$J_{NMDAR} = \gamma_i \frac{N_{NMDAR}}{\beta_{NMDAR} A_{PSD}}$$

Equation 8. The calcium flux through NMDARs. The flux is dependent on the amount of NMDARs, the area of the PSD, and channel dynamics γ_i.

$$J_{VSCC} = k_{Ca^{2+}}(Vm(t)) \cdot [VSCC] \cdot \left(e^{-\alpha_4 t} - e^{-\beta_4 t}\right)$$

Equation 9. The calcium flux through VSCC. The flux of calcium through the channels is dependent on channel density, single channel dynamics k_{Ca}, and is modulated by a biexponential based on previous studies.

Both channels are influenced by the change in membrane voltage via EPSP and BPAP:

$$V_m(t) = V_{rest} + BPAP(t) + EPSP(t)$$

Equation 10. Membrane voltage equation. Both the BPAP and EPSP are delayed biexponentials.

There is also Calcium flux out of the plasma membrane, which is given by sodium calcium exchanger (NCX) and a calcium ATP pump, PMCA. NCX harnesses the sodium electrochemical gradient, bringing in 3 sodiums in order to move one calcium against its electrochemical gradient. Extracellular sodium is also considered to be an infinite source at 2mM, and as such it is not considered in the NCX flux equation.

$$J_{NCX} = \beta_i \beta_{NCX} \left(\frac{V_{maxr22} \left[Ca_{cyto} \right]}{K_{mr22} + \left[Ca_{cyto} \right]} \right) n_{PM_r}$$

Equation 11. NCX Flux equation.

PMCA simply removes calcium from the cytosol and into the extracellular space at the cost of ATP.

$$J_{PMCA} = \beta_i \beta_{PMCA} \left(\frac{V_{maxlr23} \left[Ca_{cyto} \right]^2}{K_{mlr23}^2 + \left[Ca_{cyto} \right]^2} + \frac{V_{maxhr23} \left[Ca_{cyto} \right]^5}{K_{mhr23}^5 + \left[Ca_{cyto} \right]^5} \right) n_{PM_r}$$

Equation 12. PMCA Flux equation.

Both of these equations depend on cytosolic calcium and various constants relating to channel kinetics and protein properties. Both interact with calcium and act as buffers, which is represented by the β_i term. NCX and PMCA are distributed uniformly across the plasma membrane similar to VSCCs.

As mentioned before, there are other fixed buffers that bind calcium by the membrane. Fixed buffers are modeled via Markov kinetics like the mobile buffers. Only this time there is no diffusion component since they are membrane bound.

$$J_{B_f} = k_{B_{f,on}} \left[Ca^{2+} \right] \left[B_f \right] - k_{B_{f,off}} \left[CaB_f \right]$$

Equation 13. Fixed buffers flux equation. $[Ca^{2+}] + [B_f] \rightleftharpoons [CaB_f]$ with the forward rate constant being $k_{Bf,on}$ and the reverse rate constant being $k_{Bf,off}$.

Taken together, the plasma membrane boundary condition is:

$$-D(n \cdot \nabla [Ca^{2+}])|_{PM} = f_{in}(NMDAR, VSCC) - f_{out}(PMCA, NCX) - f_{on}(B_f)$$

Equation 14. Total plasma membrane boundary condition.
These equations remain unchanged from Bell et al.

Boundary Flux at the Neck

In addition to the boundary conditions at the plasma membrane and the endoplasmic reticulum, which act as the boundaries of the domain, we incorporated a boundary condition at the neck that was not included in the original model. This boundary condition, an outlet flux, mimics the efflux through the base of the spine neck.

The model presented in Bell et. al. treats the calcium at the base of the dendritic spine neck as a fixed concentration of 100 nM (the spine acts as an isolated system). A more physiological approach would be to include a fixed flux from the base of the neck into the dendrite proper. Following the additional boundary condition indicated in Equation 4, it has been shown that a K_N of 1 um/sec follows biological calcium transport through the dendritic spine neck[5].

$$D\nabla C * n|_N = J_N(t) = K_N C(t)|_N$$

Equation 15: Boundary condition for calcium efflux down the spinal neck. Equation from Cugno et. al.

For all of these equations, elaborations on the exact parameters/constants used and intermediary equations can be found in the supplementary material sections S1-S3.

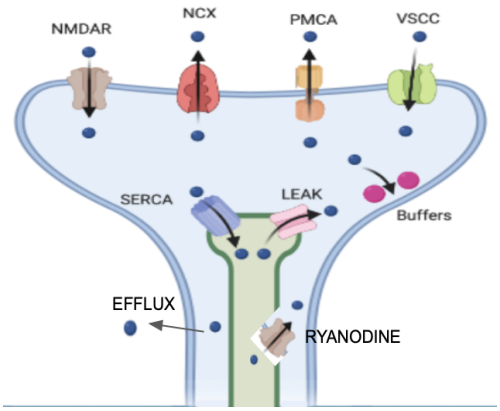

Figure 2: Diagram of the fluxes in a dendritic spine

Numerical Methods/Code

These equations were solved and modeled using COMSOL. The geometries use a fine, tetrahedral mesh. There were up to two volumes per model: the spine volume, and the SpApp volume. The basis for this project's code, the original code, was written by Bell et al., and can be found on the Rangamani Lab website. We added the extra geometries: long thin spine (with and without the SpApp) and stubby spine to the original code. We also added in the RyR dynamics based on the equations provided by Leung et al. and previous work done by Ekta Dadlani in the Rangamani Lab at the University of California, San Diego, and added the neck flux dynamics based on Cugno et al. We use the same naming convention as the original paper. A "sphere in ellipse model" is a spine with a spherical SpApp in an ellipsoidal head geometry. In total, we looked at the sphere in ellipse, sphere in sphere, sphere with no SpApp, and ellipse with no SpApp with and without our modifications (called the modified code and original code in future sections). The new geometries, the sphere in long thin model, long thin without SpApp model, and stubby model, only contain the modified neck flux and RyR. These new geometries were based on the sphere geometry. The volume of the ellipsoid and spherical models were the same at 0.06um^3, only the surface area changed[2]. Average calcium concentrations for the models were exported and graphed in MATLAB.

Results And Discussion of Results

Geometries with SpApp

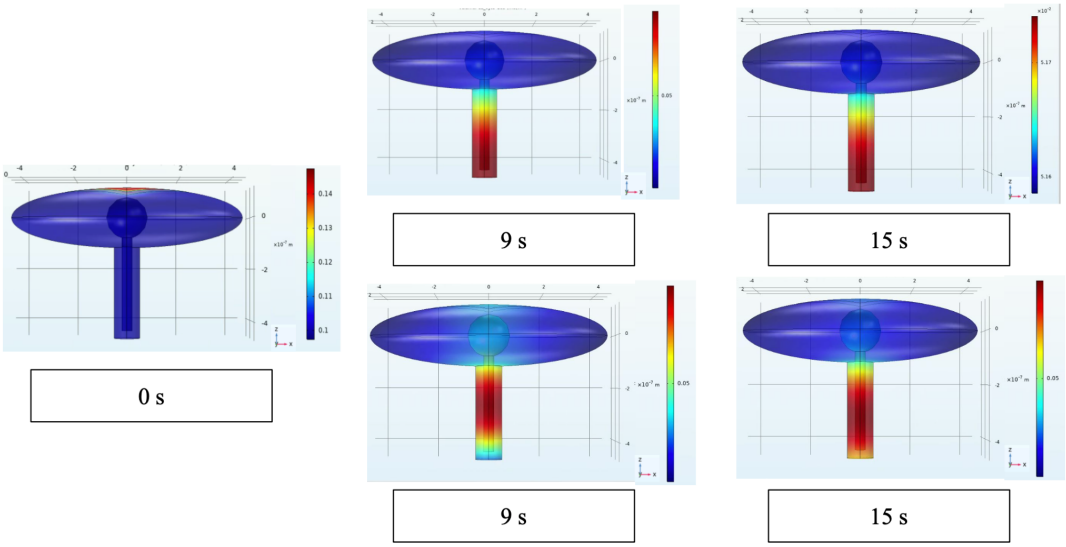

Figure 3. 3D models of a spherical SpApp in an ellipse spine at specific time stamps for both the original model and with the integration of a neck flux and ryanodine receptors. Both models had the same dynamics at 0s. The top row showcases the original model and the bottom row showcases the modified version. There is a halo of higher calcium concentration around the SpApp in the modified model, most obviously at 9s, that is not

present in the original model. Calcium slowly moves down the neck in the modified model, but not the original model, between 9s and 15s.

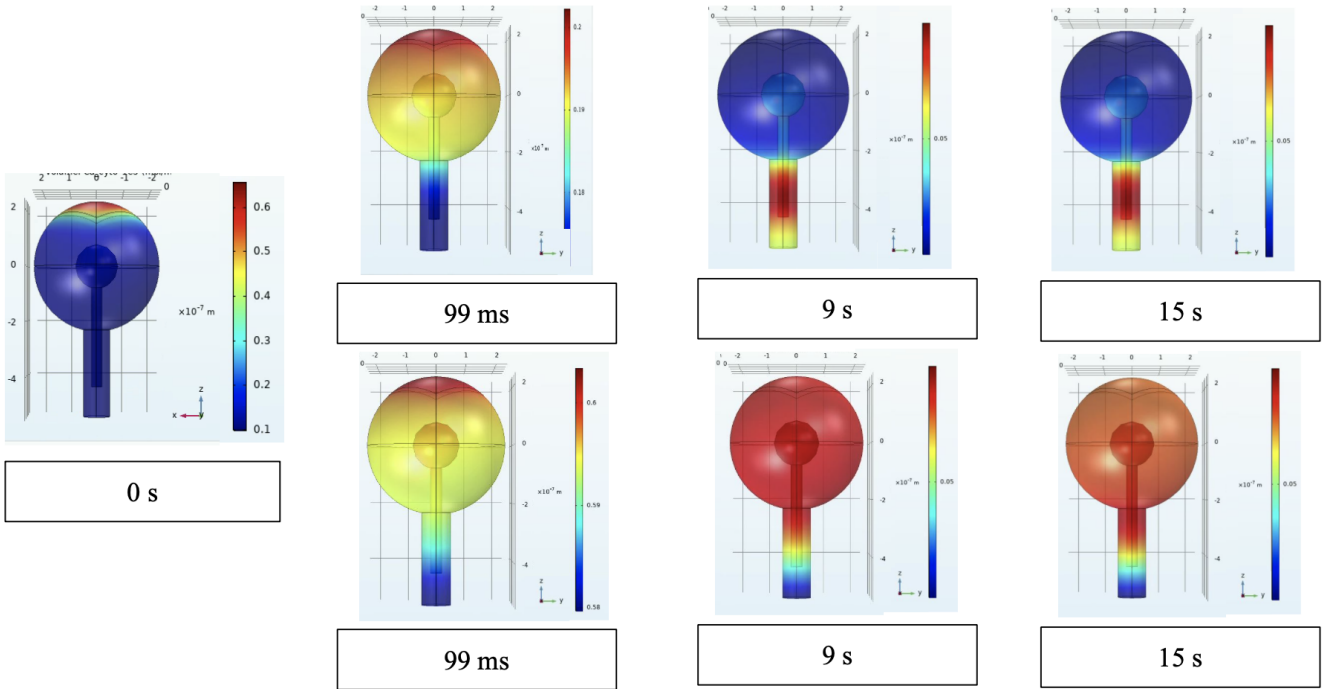

Figure 4. 3D models of a spherical SpApp in a sphere at specific time stamps for both the original model and the with integration of a neck flux and ryanodine receptors. Both models had the same dynamics at 0s. The top row showcases the original model and the bottom row showcases the modified version. There is a halo of higher calcium concentration around the SpApp in the modified model, most obviously at 99ms, that is not present in the original model. Calcium slowly moves down the neck in the modified model, but not the original model, between 9s and 15s.

From the 3D plots, we could tell that calcium quickly enters the spine head primarily through the postsynaptic density in both the modified and original cases. The ellipsoids had a larger PSD, so they had a higher initial calcium concentration at the PSD. The modified models also had a clear halo of higher calcium concentration around the spine apparatus at later times (>10ms) when compared to the original models. This halo was more noticeable in the ellipsoid geometries, as they had segments further away from the spine apparatus. Finally, there was a difference in end behavior. In some of the cases the original model, with its clamped, 0.1um calcium boundary condition, saw no change in the calcium distribution from 10s to 15s. Meanwhile, the modified model saw a very slow shift in calcium concentration towards the neck; however, the average calcium in the area is very similar. These trends can be seen in Figures 3 and 4.

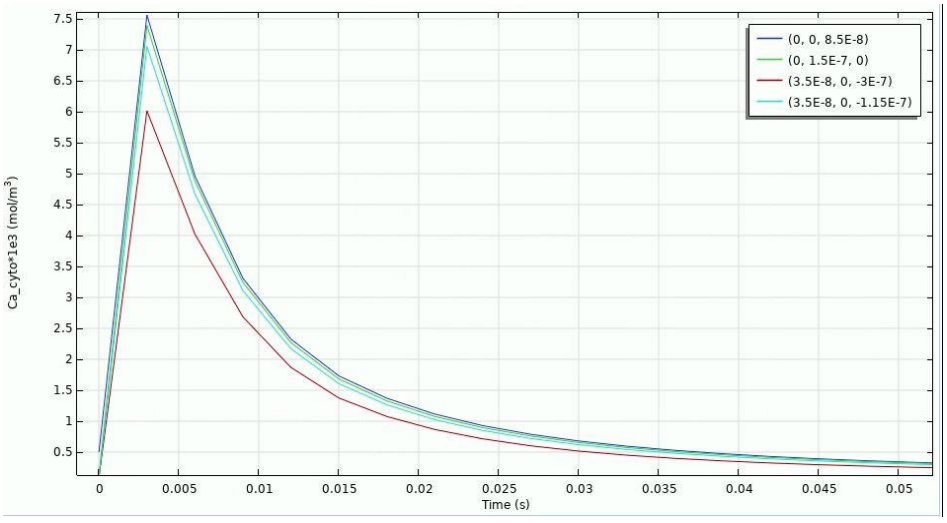

Figure 5. Amount of Calcium At 1. The top of the head, 2. the side of the head, 3. in the neck, and 4. at the interface between head and neck for the original sphere in ellipse model. In order of highest to lowest peaks: Dark blue is the top volume, green is the side volume, cyan is the head-neck interface, and red is the neck volume.

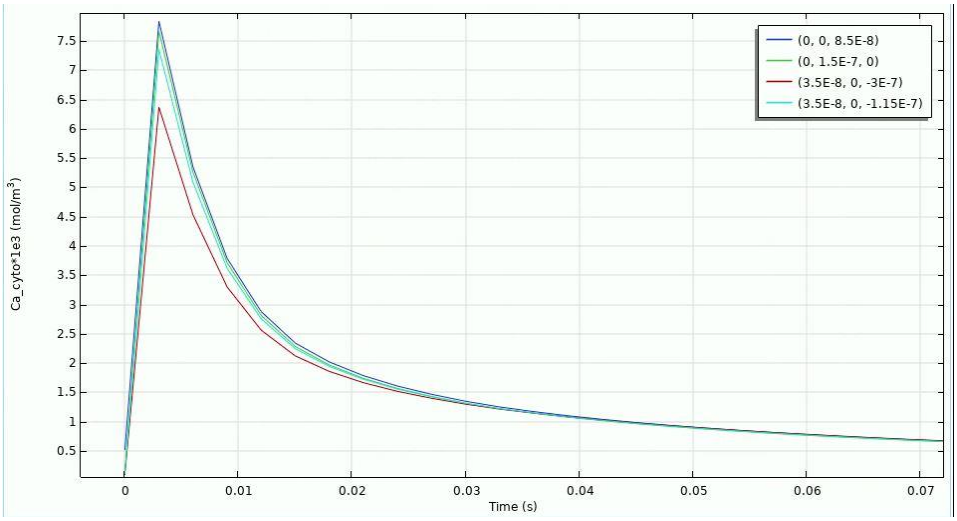

Figure 6. Amount of Calcium At 1. The top of the head, 2. the side of the head, 3. in the neck, and 4. at the interface between head and neck for the modified sphere in ellipse model. In order of highest to lowest peaks: Dark blue is the top volume, green is the side volume, cyan is the head-neck interface and red is the neck volume.

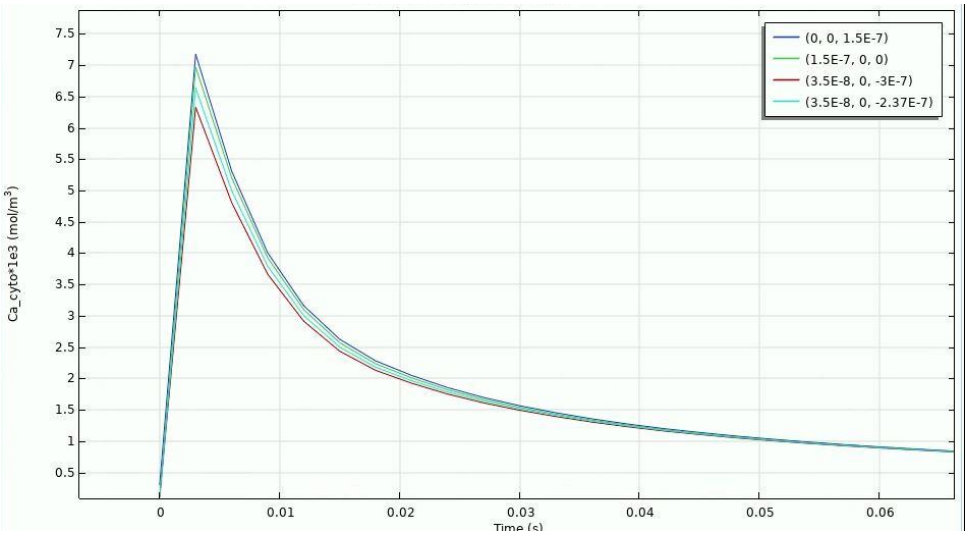

Figure 7. Amount of Calcium At 1. The top of the head, 2. the side of the head, 3. in the neck, and 4. at the interface between head and neck for the modified sphere in sphere model. In order of highest to lowest peaks: Dark blue is the top volume, green is the side volume, cyan is the head-neck interface and red is the neck volume.

These 2D graphs echo the data from the 3D plots and elaborate on the quantitative analysis. In Figures 5-7, we see a fast increase in the calcium concentration at all nodes within the first 2-3ms, and then a rapid decline afterwards which begins to slow down after ~100ms. The further the point is from the PSD, the longer it takes to reach the peak and the lower that peak is, confirming that the PSD is the major calcium source (the blue line representing the top of the head volume is always the highest, followed by green representing the side of the head volume, then cyan representing where the head meets the neck, and finally red which is inside the neck). Diagrams of where these points are in the model can be found in the supplementary materials in sections S4-S11.

Comparing the original to the modified sphere in ellipse model (Figures 5 and 6 respectively), we see there are a few key differences. First, the maxima for the modified model are higher. The peak values for the modified sphere in ellipse model are 7.94uM for the top volume, 7.82uM for the side volume, 7.44 for the interface, and 6.41 for the neck while the peak values for the original sphere in ellipse model are 7.51uM, 7.43uM, 7.06uM, 6.01uM respectively. These maxima are slightly less disparate than what we can see in the 3D models in Figure 3, potentially due to the points that were chosen. These maxima are consistently ~0.4uM different. The time to attain a peak is the same between the original and modified model, confirming the increase of slopes in the modified model. The other major difference in the models is that the time constant for the decrease in calcium is lower for the original model, which will be quantified in Table 1 below.

All 4 curves approximately converged to the same steady state value by 5s, as seen in the supplementary material in sections S4-S6. At this time point and beyond, the farther away they were from the PSD, the more calcium they had. This makes sense since calcium would be moving from the head to the neck and out. The differences between the curves after 5s were negligible (<1nM), however. It should be noted that despite the modified sphere in the ellipse model showing slow changes in the calcium concentration distribution by 15 seconds in Figure 3, both the original and modified models had similar calcium concentrations, ~0.05uM, at that time. At this time they have similar slopes of decreasing calcium concentration: -0.25nM/s with the modified models being slightly greater in magnitude. Similar dynamics/trends can be seen for the sphere in sphere model and long thin model with spherical SpApp. The exact numbers and plots are in Figure 8 and Table 1 below. Further plots are in supplementary materials sections S4-S6.

Compared to the sphere in sphere models, the sphere in ellipsoid models' peaks for the neck region were much lower than the other 3 peaks, as seen when comparing Figures 6 and 7. This indicates that the calcium may have been trapped in the head for longer (and exposed to the sinks in the head) before making its way into the neck.

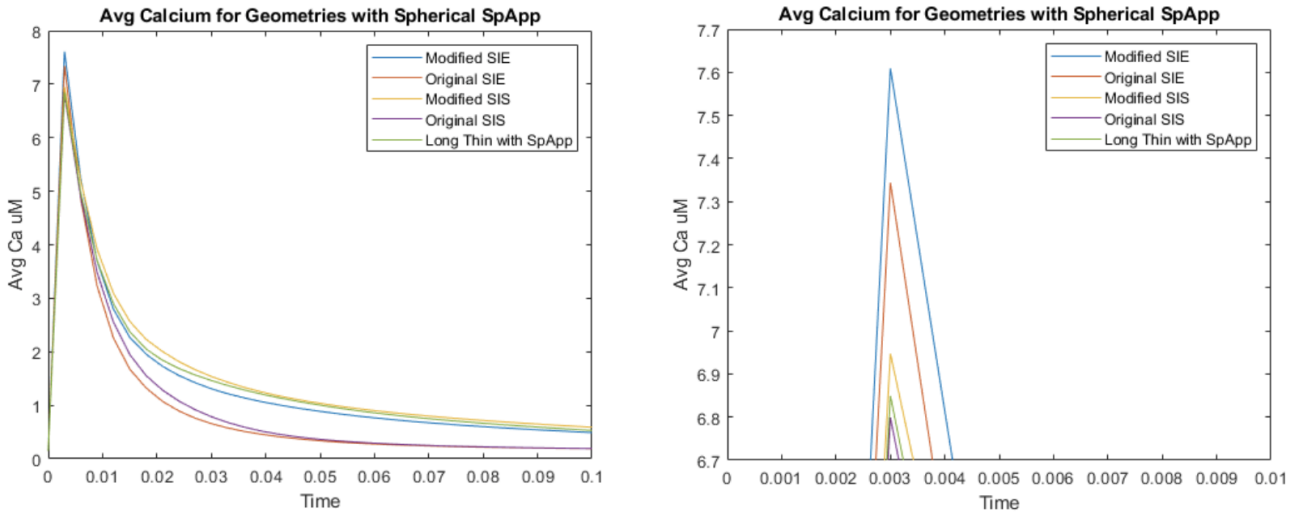

Figure 8. Graphs for Average amount of calcium throughout the spine volume (excluding the SpApp) for the All Spherical SpApp geometries. The graph on the right zooms into the peaks from the graph on the left. Trends are quantified in Table 1.

Model	Peaks: Original, Modified*	Time Constant: Original, Modified*
Sphere in Sphere	6.80uM, 6.95uM	9.1ms, 11.67ms
Sphere in Ellipse	7.34uM, 7.61uM	7.44ms, 8.59
Long Thin with SpApp	6.85uM*	9.5ms*

*The long thin model only has a modified version of the model

Table 1. Comparison of calcium peaks and time constants of peaks in three different spine geometries with the implementation of the Neck flux & Ryanodine receptor flux (modified) and without (original).

Based on Figure 8 and Table 1, it was clear that the ellipsoid models had a higher calcium peak at 2-3ms than the spherical models. It was also clear that the modified models had higher peaks than their corresponding unmodified versions. Furthermore, assuming the curves are exponential, the descending time constant was higher in the spheres when compared to ellipsoids, and was higher in the modified version compared to their respective unmodified version. The higher peaks along with lower time constants for the ellipsoid geometry compared to spherical geometry is likely due to the increased surface area both for inwards and outwards calcium flux through the plasma membrane[2]. This matches results obtained by Bell et al. The increased peaks and lower decaying time constants for the modified models when compared to the original ones is most likely due to the input of calcium via CICR. The long thin model had a similar peak to the sphere model, likely due to its spherical head, but had a time constant that was closer to the ellipsoid model, likely due to its greater surface area for calcium to leave.

Neck Flux

We quantified the effect of the neck flux on the model. We compared a sphere in ellipse geometry of the original model against a model that only had our neck flux added and no RyR. The neck flux makes a small change in the internalization of calcium.

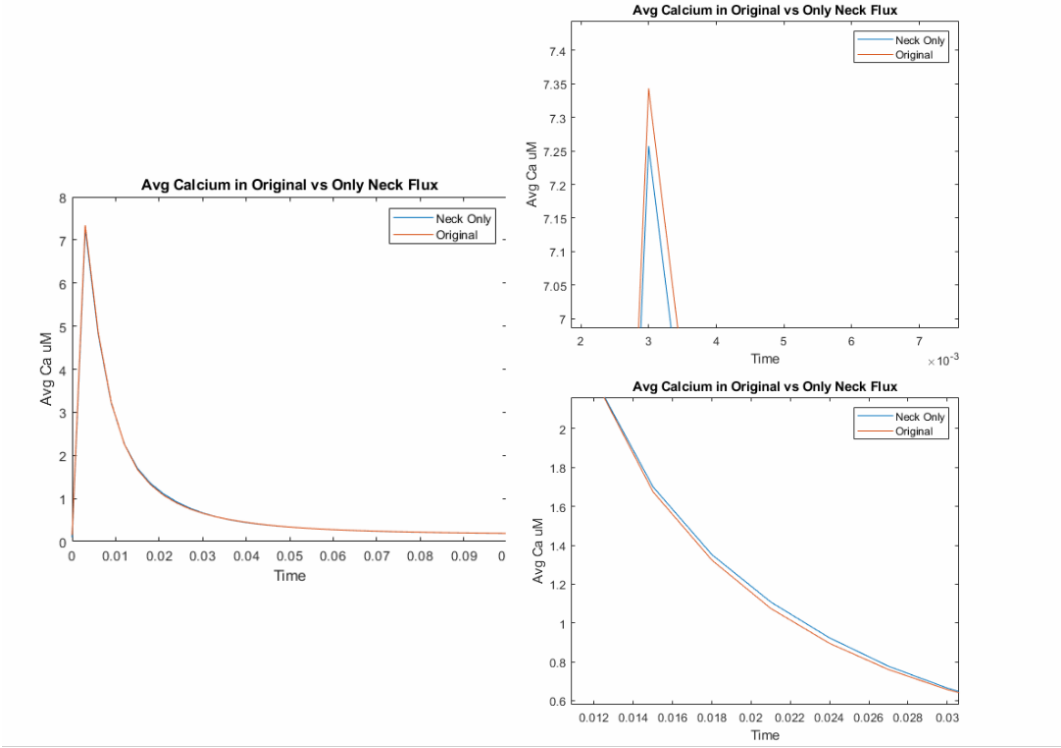

Figure 9. Comparison of original model to a modified model with only the neck flux, but no added RyR to the SpApp. This is for the sphere in ellipse geometry. The graph on the top zooms into the peak of the graph on the left, while the bottom graph zooms into the curve indicating different time constants.

Based on Figure 9, there is a reduction in the peak calcium concentration from 7.34uM to 7.25uM between the original and modified model with only neck flux. The decaying time constants were 7.51ms for the modified and 7.01ms for the original. Though this value is small, it is still significant since the original concentration of calcium is 100nM. Calcium secondary messenger pathways are very sensitive to intracellular calcium levels, and even small differences can change how the synapse evolves. The neck flux initially induces faster calcium depletion, but then slows down the depletion as calcium concentration falls. This makes sense since the experimental neck flux was dependent on the calcium concentration, accounting for convection due to increased calcium concentration. Increasing the neck flux coefficient only incrementally changes these values, however. This is likely because the concentration at the neck is fairly low, which indicates that not much calcium actually leaves through the neck.

SpApp vs No SpApp

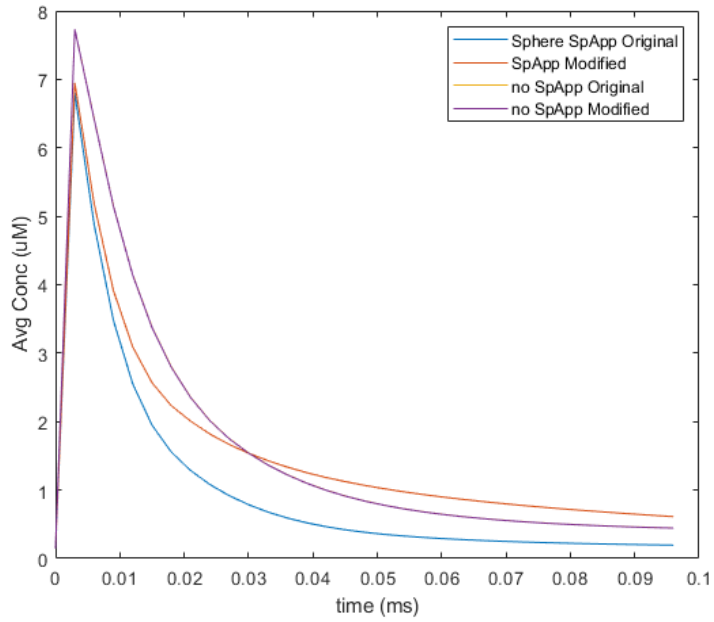

Figure 10. Graph of Average Calcium Concentration in the cytosol of the spine for 4 different models. Original and Modified models of a spherical SpApp (blue and red respectively) and spherical head, as well as the original and modified versions of spherical heads without a SpApp (yellow and purple respectively). At low time-scales yellow and purple overlap. Pertinent values are in Table 2

Model	Peak (Original, Modified)	Time Constant (Original, Modified)
Sphere in Sphere	6.799 uM, 6.947 uM	9.1 ms, 11.7 ms
Spherical Head without SpApp	7.729 uM, 7.727 uM	14.6 ms, 14.6 ms

Table 2. Comparison of Calcium peaks and time constants of peaks in sphere spine geometry with a SpApp and without a SpApp.

Without the SpApp, the only difference between our model and the original model is the neck flux, as the RyR are localized entirely on the SpApp. Many of the same trends from the SpApp models hold for the models without a SpApp. Calcium primarily entered through the PSD at time 0, leading to fast accumulation and then depletion that slowed down over time (3D figures in the supplementary material in sections S8-S10). Based on Figure 10 and Table 2, the cases without a SpApp had a higher peak concentration than the cases with a SpApp. This likely indicates that the SpApp acted more as a calcium sink in shorter timescales, consistent with RyR taking 10-100ms to activate. At longer time-scales, the modified SpApp would act as a source of calcium and maintain a higher average calcium concentration in the spine cytosol compared to the models without a SpApp. It also should be noted that the concentration of calcium in the cytosol would initially decrease faster in the SpApp present cases (lower time constant), consistent with the SpApp acting as a sink in shorter timescales before becoming a source, which is consistent with the Bell et. al paper. The unmodified SpApp only acted as a sink and led to both a lower peak and lower average calcium concentrations at all times. Of note, in the sphere without SpApp, the modified model with neck flux did have slightly lower peak calcium levels. This matches the neck flux test from Figure 9, in which the version with a neck flux had a lower peak without RyR involvement. The difference in this case is much smaller, however. It is only 2nM compared to the 100nM difference in the neck flux test, and could just be due to computational artifacts.

Discussion: Limitations of Original Model and Review of Relevant Results

In this report, we expanded Bell et. al's model of an isolated, single dendritic spine of a rat hippocampal area CA1 pyramidal neuron with the addition of two flux sources: the efflux of Ca^{2+} from the neck of a dendritic spine and the flux of Ca^{2+} from the spine apparatus to the cytosolic region through ryanodine receptors. We consider a longer timescale of 10-15 seconds to incorporate the spine neck's ability to act as a boundary

condition for the flux of calcium. Similar to the original model, we do not consider the calcium dynamics in the mitochondria (a calcium store) because the mitochondria are located on the outside of the dendritic spine. We do not consider the addition of the IP_3 receptors in our expanded model, because the dynamics of the IP_3 receptors are dependent on the physical Mitochondria and Endoplasmic Reticulum Contact Sites (MERCs)[12]. We also do not consider α-amino-3-hydroxy-5-methyl-4-isoxazolepropionic acid receptor, or AMPAR. AMPAR could act as a calcium flux into the cell. However, it is primarily a sodium channel, not a calcium channel. Furthermore, its contributions are tied to learning and memory, and as such are both rapidly modified in the ms range and modified in the second-hours range for long term potentiation. Because of these factors, they were not included in this model.

The inclusion of the neck flux was to model how the spine can connect to the rest of the dendrite proper. The original model code either clamped the neck flux at 0.1uM or treated it as an isolated system. Neither capture how calcium actually exits the dendritic spine system, which can have implications on dendritic signaling cascades. The inclusion of RyRs was to better model how the SpApp, which has been shown to have RyRs throughout the spine head and neck, will influence calcium dynamics in the spine[15]. This was a further improvement from the calcium sink generalization used in the original model.

The neck flux alone had subtle effects on calcium dynamics. Based on Figure 3 and 4, post 10s, the models with neck flux could show more calcium exiting the spine head, albeit at very slow speeds. Models with neck flux could also have lower peak calcium concentrations, but higher decaying time constants for the average calcium transient. While the changes are small, secondary messenger pathways involving calcium are very sensitive to intracellular calcium concentration, which starts off at 100nM. Less peak calcium that persists for longer can have downstream effects. Of note, this phenomenon was seen in the sphere in ellipse case. There were almost no differences in the sphere without SpApp case between the modified and unmodified versions (the only difference between the modified and unmodified sphere without SpApp would be the neck flux since RyR was only on the SpApp). This could indicate that spines with a SpApp interact with the rest of the dendrite in a different way than spines without a SpApp, even without considering CICR. The subtle effect of the neck flux addition does make sense considering that it is based on calcium concentration at the neck, which was always lower than the concentrations at the head based on Figures 5-7. These results confirm that these spine models are naturally isolated, and it would take the summation of many spines to cause a large change in calcium concentration in the dendrite proper.

The addition of RyRs had great effects on the calcium dynamics. There was a clear increase in peak calcium concentration and longer decay time constants between the original (without RyR or neck flux) and modified models that included SpApps based on Figure 8. These changes represented themselves in the 3D models as halos of increased calcium concentration around the SpApp that persisted through the seconds timescale. The halos were not present in the original model (Figures 3 and 4). We then compared the models with a SpApp to models without a SpApp. The models without a SpApp actually had higher peaks than the ones with a SpApp, regardless of whether the SpApp had RyR on it or not (Figure 10/Table 2). This confirms that RyR successfully had a slower activation time than the other boundary condition fluxes. Further supporting this conclusion is that the models without a SpApp had longer decay time constants than the ones with a SpApp (since decay constants were within the first 15ms), but, after 30-40ms, the modified models with SpApp had higher average calcium concentrations, most likely due to CICR. These results give biological insight for both the localization of calcium in dendritic spines and a clearer picture of the role of the SpApp in the spines. It acts as primarily a sink in the first 10ms, then becomes a source, and then switches back to being a sink as calcium leaves the system and quells CICR. The fact that models with RyR on the SpApp showed higher peaks compared to the original models without RyR on the SpApp does indicate that RyR has partial release before it is fully activated, it is just outpaced by SERCA pumps in that time frame.

These additions did not come at the cost of the original conclusions from the paper, as we saw many of the same trends. There was an initial sharp spike in cytosolic calcium that was quickly depleted by the SpApp and plasma membrane acting as a sink. This led to a steep decline in cytosolic calcium and a relatively slow propagation of calcium down the spine neck. The progression of calcium in our modified and the original model followed a nonlinear nature. Even with the modifications, the comparisons between the spherical and ellipsoidal head geometry remained the same from Bell et al. Ellipsoid geometries generally had faster calcium intake followed by faster calcium depletion due to having a higher surface area for plasma membrane flux, reinforcing the importance of surface area to volume ratio in the spine. Greater head surface area also meant

less calcium got into the neck (based on Figures 3-5), meaning that larger spines were even more isolated from the dendrite proper, and thus could have more local calcium responses.

Lastly, we presented novel geometries. They showed the same general trends, namely, that of a sharp spike in cytosolic calcium stemming from the PSD that rapidly decayed up to ~100ms then continually slowed down. Based on Figure 8 and the supplementary material in sections S6-S7, the long thin geometry had calcium dynamics that fell between those of the spherical head and ellipsoid head, both for the case with and without SpApp. The initial intake of calcium and subsequent calcium peak was similar to the spheroidal models, but the time constants were closer to the ellipsoidal geometries, meaning less calcium came into the spine than the ellipsoid geometries, but the calcium in the spine persisted for longer than the ellipsoidal geometries. The stubby geometry (supplementary section S10) had a similar peak value and time to peak to that of the sphere without SpApp (7.73uM vs 7.80uM at 2-3 ms respectively), but a longer time constant of 16.7ms vs 14.6ms respectively. This is despite there being much less distance between the PSD and neck flux, which confirms that calcium activity is largely isolated in the spine head in these models. It is possible that the increase in average calcium in the stubby compared to the other geometries is what lets it grow, as more calcium has been correlated to spine growth[11].

Conclusion

The changes we made to the original model by Bell et al. revealed several interesting aspects about dendritic spines. The first aspect is that the spine apparatus's role in calcium activity within the spine evolves over the time course of the calcium transient. It initially acts more as a sink, then later on as a source as the RyRs amp up their response to the influx of calcium, and then goes back to being a sink once RyRs close. It also gives insight to where a greater concentration of cytosolic calcium is localized within the spine, as there were consistently higher calcium levels around the SpApp when compared to the membrane. The second aspect was that we were able to confirm that the spine head is very isolated in terms of calcium activity. In the original model we were only able to speculate that, but with a proper neck flux term it is clear that very little calcium makes it out of the head and into the dendrite proper. This could indicate that secondary messenger pathways responding to calcium flow from the spine's SpApp and plasma membrane almost entirely take place within the head. Lastly, we were able to reinforce the conclusions from Bell et al. that the dominant force in cytosolic calcium concentration is surface area to volume ratio, and as such, smaller spines, like the stubby geometry, will naturally tend to grow due to their ability to hold more calcium per stimulus.

Taking a broad review of the knowledge our modified model incorporates and the biological features it adds (ie neck flux, SpApp as a source), we can firmly conclude that the new model is an improvement from the original. That being said, there are many other aspects of dendritic spines that can be implemented to make the model even more biologically accurate.Once again the SpApp geometry is greatly simplified, and could be changed to better follow realistic folded, haphazard geometries[2]. It is also possible to add actin convection to the system. When calcium enters the spine, there is myosin-actin excitation contraction coupling, much like there would be in muscles[11]. This would require a model that can support changing the spine shape and size as calcium enters, but would give more realistic calcium flow and is perhaps the way calcium can leave the spine and enter the dendrite proper, as diffusion alone does not seem to be enough to induce steady calcium flow through the neck. Looking at other head and neck geometries can also give insight on how different spines can induce synaptic plasticity and interact with presynaptic neurons. Finally, the current model never returned to the 100nM starting cytosolic calcium concentration. It reached ~50nM and continued to decrease by 15s. Modifications in the leak channel formulas or additions of new fluxes might be needed to compensate for this.

References:

1. Basnayake K, Mazaud D, Bemelmans A, Rouach N, Korkotian E, et al. (2019) Fast calcium transients in dendritic spines driven by extreme statistics. PLOS Biology 17(6): e2006202. https://doi.org/10.1371/journal.pbio.2006202
2. Bell, Miriam, et al. "Dendritic spine geometry and spine apparatus organization govern the spatiotemporal dynamics of calcium." Journal of General Physiology 151.8 (2019):
3. Berridge, Michael. (2002). The endoplasmic reticulum: A multifunctional signaling organelle. Cell calcium. 32. 235-49. 10.1016/S0143416002001823.
4. Breit, Markus, and Gillian Queisser. "What is required for neuronal calcium waves? A numerical parameter study." *The Journal of Mathematical Neuroscience* 8.1 (2018): 1-22.
5. Cugno, A., Bartol, T.M., Sejnowski, T.J. et al. Geometric principles of second messenger dynamics in dendritic spines. Sci Rep 9, 11676 (2019).
6. Fill M, Copello JA. Ryanodine receptor calcium release channels. Physiol Rev. 2002 Oct;82(4):893-922. doi: 10.1152/physrev.00013.2002. PMID: 12270947.
7. Futagi, D., Kitano, K. Ryanodine-receptor-driven intracellular calcium dynamics underlying spatial association of synaptic plasticity. *J Comput Neurosci* 39, 329–347 (2015). https://doi.org/10.1007/s10827-015-0579-z
8. Higley, Michael J, and Bernardo L Sabatini. “Calcium signaling in dendritic spines.” *Cold Spring Harbor perspectives in biology* vol. 4,4 a005686. 1 Apr. 2012, doi:10.1101/cshperspect.a005686
9. Holcman, David, Z. Schuss, and Eduard Korkotian. "Calcium dynamics in dendritic spines and spine motility." Biophysical journal 87.1 (2004): 81-91.
10. Keizer, J, and L Levine. “Ryanodine receptor adaptation and Ca2+(-)induced Ca2+ release-dependent Ca2+ oscillations.” *Biophysical journal* vol. 71,6 (1996): 3477-87. doi:10.1016/S0006-3495(96)79543-7
11. Korkotian, Eduard, and Menahem Segal. "Release of calcium from stores alters the morphology of dendritic spines in cultured hippocampal neurons." *Proceedings of the National Academy of Sciences* 96.21 (1999): 12068-12072.
12. Leung, A., et al. "Deciphering the postsynaptic calcium-mediated energy homeostasis through mitochondria-endoplasmic reticulum contact sites using systems modeling." *bioRxiv* (2020)
13. Lu, Ju, and Yi Zuo. “Clustered Structural and Functional Plasticity of Dendritic Spines.” *Brain Research Bulletin*, Elsevier, 13 Sept. 2016, https://www.sciencedirect.com/science/article/abs/pii/S0361923016302544?via%3Dihub.
14. Risher WC, Ustunkaya T, Singh Alvarado J, Eroglu C (2014) Rapid Golgi Analysis Method for Efficient and Unbiased Classification of Dendritic Spines. PLoSONE 9(9): e107591. doi:10.1371/journal.pone.0107591
15. Roderick, H. Llewelyn, Michael J. Berridge, and Martin D. Bootman. "Calcium-induced calcium release." *Current Biology*13.11 (2003): R425.
16. Segal, Menahem, Andreas Vlachos, and Eduard Korkotian. "The spine apparatus, synaptopodin, and dendritic spine plasticity." *The Neuroscientist* 16.2 (2010): 125-131.
17. Spacek, Josef, and Kristen M. Harris. "Three-dimensional organization of smooth endoplasmic reticulum in hippocampal CA1 dendrites and dendritic spines of the immature and mature rat." *Journal of Neuroscience* 17.1 (1997): 190-203.
18. Yadav, Aniruddha et al. “Morphologic evidence for spatially clustered spines in apical dendrites of monkey neocortical pyramidal cells.” *The Journal of comparative neurology* vol. 520,13 (2012): 2888-902. doi:10.1002/cne.23070